NUMERICAL SIMULATION OF PRESSURE RECOVERY PHENOMENON IN LIQUID AMMONIA TANK

Srinivas Sivaraman, Dmitriy Makarov, Vladimir Molkov*
HySAFER Centre, Ulster University, BT37 0QB, Newtownabbey, UK
corresponding author: sivaraman-s@ulster.ac.uk

ABSTRACT

A phase transition develops when a pressurised ammonia vessel is vented through a relieve valve or as a result of shell cracking. Significant pressure recovery in the vessel can occur as a consequence of this phase transition following initial depressurisation and may lead to complete vessel failure. It is critical for safety engineering to predict the flash boiling behaviour and pressure dynamics during the depressurization of liquid ammonia tank. This research aims to develop and compare against available experimental data a CFD model that can predict two-phase behaviour of ammonia and resulting pressure dynamics in the storage tank during its venting to the atmosphere. The CFD model is based on the Volume-of-Fluid (VOF) method and Lee evaporation/condensation approach. The numerical simulation demonstrated that liquid ammonia, which is initially at equilibrium state, begins to boil throughout due to the decrease of its saturation temperature with the pressure drop during tank venting. In order to understand phenomena underlying the pressure recovery, this paper analyses dynamics of superheated ammonia formation, its swelling, vaporisation, contribution to gaseous ammonia mass and volume in ullage space and gaseous ammonia venting. Performed in the study quantitative analysis demonstrated that the flash boiling, and gaseous ammonia produced by this phase change were the major reasons behind the pressure recovery. The simulation results of flash boiling delay accurately matched the analytical calculation of bubble rise time. The developed CFD model can be used as a contemporary tool for inherently safer design of ammonia tanks and their depressurisation process.

NOMENCLATURE:

Latin

C_p	*Specific heat capacity* $(J/kg/K)$
$\vec{F}$	*Body force term* (N/m^3)
g	*Acceleration due to gravity* (m/s^2)
H	*Height (m)*
h	*Sensible enthalpy* $(J/kg/K)$
k	*Thermal conductivity* $(W/m/K)$
L	*Latent heat of evaporation/condensation (J/kg) or length (m)*
M_W	*Molecular weight (kg/kmol)*
$\dot{m}_{lg}$	*Mass rate of evaporation* $(kg/s/m^3)$
$\dot{m}_{gl}$	*Mass rate of condensation* $(kg/s/m^3)$
$\dot{m}$	*Mass rate of phase transition* $(kg/s/m^3)$
M_U	*Ullage mass (kg)*
P	*Pressure (Pa)*
R	*Universal gas constant, R=8314* $(J/kmol/K)$
r	*Mass transfer intensity parameter* (s^{-1})
S_E	*Source term in energy equation* $(J/s/m^3)$
T	*Temperature (K)*
T_{sat}	*Saturation temperature (K)*
U_{bubble}	*Bubble rise velocity (m/s)*
V_U	*Ullage volume* (m^3)
$\vec{v}$	*Velocity (m/s)*
W	*Width (m)*
y	*Species mass fraction (-)*

Greeks

α	*Volume fraction (-)*
μ	*Molecular viscosity* $(kg/m/s)$
ρ	*Density* (kg/m^3)
σ	*Surface tension coefficient (N/m)*

Subscripts

air	*Air*
g	*Gas phase*
l	*Liquid phase*
NH3	*Ammonia*
t	*Turbulent*

1. INTRODUCTION

Ammonia has been proven as the most promising hydrogen carrier owing to its high energy density, significantly higher volumetric and gravimetric hydrogen densities compared to other carriers [1]. Ammonia is stored and transported as a liquid at meta-stable condition either by compressing under high pressure at ambient temperature or under atmospheric pressure and temperature of -33.5 ℃. It is vital to depressurise the system in emergency situations in a way to exclude damage to the pressure vessel. Over-pressurisation of pressure vessels is the worst-case incident scenario [2], which can lead to catastrophic vessel rupture and cause significant harm to people, property, nature, and the built environment. There have been incidents where liquid ammonia storage tanks were over-pressurized, causing massive loss, such as the 1976 catastrophic rupture of a tanker carrying 19 tonnes of liquid ammonia in Houston, USA [3]. This kind of incident scenarios needs to be properly evaluated and preventive engineering procedures developed.

When pressurised liquid is subjected to depressurisation, the liquid is suddenly super-heated and undergoes a rapid phase change [4]. Such rapid phase change process, i.e. flash boiling, can result in significant re-pressurization of the system which may lead to a complete failure of the storage tank. In the past quite a few papers focused on the flash boiling phenomenon due to sudden depressurisation, examples of those for liquid nitrogen (LN2) include [4–7], water [8,9], refrigerants [10], cryogenic liquids used as coolants in nuclear reactor and space applications [11,12], and liquid hydrogen (LH2) [13]. Summary of the previous findings is briefly presented below.

In 1983, Boeing Airspace conducted blowdown experiments [7] to comprehend the flashing phenomena of LN_2 under depressurisation rates of 0.1 to 0.4 ullage volume per second. The authors concluded that depressurization rate had a significant impact on the pressure recovery pattern and that the presence of artificial nucleation sites decreased the pressure drop at which flash boiling was initiated (i.e. pressure undershoot). Other experiments focusing on LN_2 flashing [4–6] confirmed this conclusions and demonstrated that the pressure recovery dynamics is influenced by factors such as saturation and stratification of liquid. The blowdown experiment for LN_2 by Watanabe et. al in 1998 [6] investigated the formation of mist layer under higher depressurisation rates ranging between 0.01 to 4 MPa/s. The authors hypothesized that mist layer formation is an important phenomenon influencing the thermal non-equilibrium states during flash boiling and concluded that mist layer became denser with increasing rate of depressurisation in the study.

Experimental tank depressurisation study conducted for refrigerant R-22 [10] in two vessel geometries, 250 mL steel vessel and 75 mL glass tube, demonstrated that flash boiling behaviour and associated pressure recovery characteristics was dependent on the initial storage pressure, vessel material and geometry, and initial liquid fill level. The authors claim that in the case of steel tanks, heterogeneous boiling from the tank sides predominated. In contrast, the initial storage pressures before tank depressurization determined the boiling mechanism in the case of a glass tube. For lower initial pressures, self-sustained flash evaporation throughout the liquid bulk dominated the process, while for higher initial pressures, heterogenous boiling from the side walls dominated the process. Influence of liquid level on the depressurisation dynamics was investigated by several authors [8,9,12,13] and proved that initial liquid fill level had a significant impact on the pressure recovery characteristics. In 2005, Saury et. al [8] through their blowdown experiment of pressurised water storage systems concluded that violence of flash boiling, time taken to trigger flash boiling due to pressure drop (i.e. boiling delay) and the evaporated mass were linearly increasing function of initial liquid height. They also demonstrated that boiling delay decreases with increased rate of depressurisation.

The large-scale experiment performed for investigating the depressurisation and flash boiling in 30 m^3 LH_2 tank [13] demonstrated that the pressure recovery is observed only for high initial liquid fill level and similar phenomenon is not observed with lower initial fill levels. In the experiment, high temperatures of gaseous hydrogen (250 K) were observed at the top of the tank, which is orders of magnitude higher than the liquid hydrogen temperature. The reason for this high temperature gas presence inside thermally isolated cryogenic tank remains unclear. The authors also developed a CFD

model to numerically predict the phenomenon, however, the in-house CFD code did not include condensation as a part of the phase change simulation and the authors hypothesised that this could be the reason for model's significant over-estimation of the pressure recovery pattern. Additionally the authors had used laminar model and considered incompressible liquid for simplicity of simulation.

In 2022, Qiuju Ma et al. [14] developed a CFD model for studying the rupture of 46 L LPG tank at initial pressure of 2.2 MPa abs and the associated explosive boiling behaviour. The pressure recovery was simulated during the rupture of the storage tank but the model under-predicted pressure peak during recovery period by 15.8% compared to the experimental data. The authors had hypothesized that this under-prediction could be due to the inability of the VOF to capture the bubble generation or collapse during the transient depressurisation period.

In 2022, Tian et al. [15] undertook an experimental study on depressurisation of superheated water both pure and containing ethanol impurities. The results showed that the increase of impurities resulted in more rigorous boiling and the pressure recovery observed was highest for 3.5% ethanol content. Increase of ethanol content more than this value resulted in decrease of pressure recovery ratio.

Understanding of the heat and mass transfer in two-phase media during storage tank depressurisation and its influence on flash boiling phenomenon are pivotal for development of efficient prevention and mitigation measures against over-pressurisation of cryogenic and pressurised storage vessels. In this context, the availability of predictive models for inherently safer depressurisation of liquid ammonia tanks is crucial given the growing interest in ammonia's use as a hydrogen carrier and potential fuel for marine vessels. To the best of author's knowledge, no research has been published to comprehend the pressure recovery dynamics and flash boiling behaviour during tank venting operation in liquid ammonia storage systems. This study aims at the development of a multiphase CFD model for investigating the flash boiling of highly pressurised liquid ammonia tank when subjected to tank venting operation, including boiling/condensation, to enable the accurate prediction of pressure recovery phenomenon (PRP). This understanding helps in predicting safer depressurisation rates to prevent catastrophic damage to the liquid ammonia storage tanks due to flash boiling.

2. EXPERIMENT WITH PRESSURISED LIQUID AMMONIA TANK

The large-scale ammonia dispersion experiment conducted at INERIS [16] was used in this paper for comparison with the simulation results of liquid ammonia tank depressurisation. The experimentalists used three 12 m^3 horizontally located cylindrical pressurised liquid ammonia storage tanks for 15 tests. For each test only one of the three storage tanks was connected to the release system with nozzle. The schematic of the experimental set-up is shown in Fig.1. Each of the tanks was 4.81 m in total axial length with internal length of 3.7 m and internal tank diameter of 1.874 m. The ammonia vapour pressure was monitored by sensor located in the upper part of the tank.

A 10.4 m long flexible pipe with 50 mm internal diameter was used to connect the 3/2-inch bore diameter manual valve on the tank to the release system. The release system included a 1.37 m long pipe with internal diameter of 50 mm instrumented with valve, pressure sensor, thermocouples and release nozzle. The release nozzle consisted of different configurations depending on the test, including release through flanges, different orifice diameters and downward oriented jet. Test No.1 selected for this numerical study was designed for release of gaseous ammonia from the vapour head of the tank for which the release orifice configuration consisted of a 0.19 m long pipe with a 50 mm diameter release nozzle maintained horizontally 1.015 m above the ground level. With this setting, the release nozzle is positioned around 12.2 m away from the storage tank external shell.

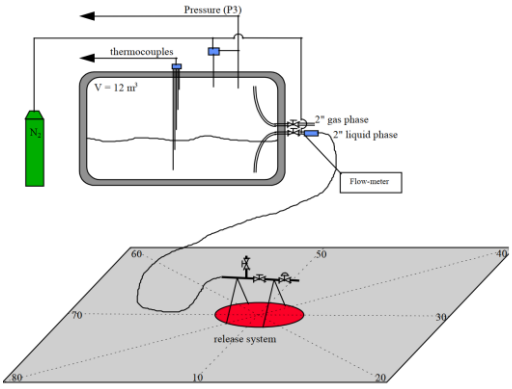

Figure 1. Schematic of the experimental set-up [16]

The experimentalists reported that variations in atmospheric conditions between daytime and night-time influenced the liquid ammonia temperature and internal pressure prior to release tests [16]. In this work, the authors assumed that the liquid ammonia's initial temperature in the tank was 9.5°C. This assumption was made through reverse engineering and comparing simulation findings with experimental data. This is less than the mean ambient temperature of 14°C that was experimentally recorded at the time of release in experiment but given the previously indicated variation in daytime and night-time temperatures, it is a reasonable assumption. The test was stopped when the ammonia vapour pressure dropped to approximately 0.18 MPa abs, the time taken for this venting period was reported as 460 s. The amount of ammonia released during 460 s in this test was reported to be about 300 kg. Due to problems with measuring device the mass flow rate was not reported by the authors for any of the experimental trials [16]. The experimental results of Test No.1 on dispersion in the atmosphere will be used in our follow-up study to assess the CFD model predictive capability to estimate hazard distances defined by ammonia toxicity and flammability limits.

3. TWO PHASE CFD MODEL

3.1. Governing equations

Three dimensional multiphase CFD model solves conservation equations for mass, momentum, energy and ammonia mass fraction. The RANS approach to turbulence simulation with SST k-ω model is adopted as it allows turbulence damping which is critical for capturing instabilities in interfacial cells in boiling flows [17]. The Volume of Fluid (VOF) model is applied for simulation of liquid and gaseous phases interaction and described in detail below.

3.2. VOF model equations

The Volume of Fluid model is used in the present study for simulation of flash boiling and pressure recovery. It belongs to Euler-Euler class models typically used for fluid-fluid flows and is based on homogenous equilibrium model (HEM) which assumes equilibrium between liquid and gas phase velocities and temperatures. This is the preferred model for liquid-vapor interface tracking and has been widely used in literatures for boiling flows, see for example [18,19]. It is also the preferred method considering its low computational cost; performing full Eulerian multiphase simulations with non-homogenous treatment of phases' velocities and temperatures wouldn't be affordable in the considered case.

In the VOF model, the momentum and energy equations are shared between the phases and the volume fraction (α) of all phases in each control volumes sums up to unity, $\alpha_g + \alpha_l = 1$. In this study, the gas phase contained mixture of ammonia vapour and air, and liquid phase consisted of liquid ammonia. The volume fraction equation as shown in Eq. (1) is solved for the liquid phase while for the gas phase the volume fraction is calculated using constraint given in Eq. (2):

$$\frac{\partial}{\partial t}(\alpha_l \rho_l) + \nabla(\alpha_l \rho_l \vec{v}_l) = \dot{m}_{lg} - \dot{m}_{gl}\,, \tag{1}$$

$$\alpha_g = 1 - \alpha_l. \tag{2}$$

A single momentum conservation equation is solved through the computational domain and the velocity in a control volume is shared between the liquid and vapour phases:

$$\frac{\partial}{\partial t}(\rho\vec{v}) + \nabla \cdot (\rho\vec{v}\vec{v}) = -\nabla P + \nabla \cdot \left((\mu + \mu_t)(\nabla\vec{v} + \nabla\vec{v}^T) - \frac{2}{3}(\mu + \mu_t)(\nabla \cdot \vec{v})I\right) + \rho\vec{g}. \tag{3}$$

The momentum Eq. (3) is solved depending on all the phases involved in the model contributing through their properties such as density ρ and viscosity μ, which are calculated based on their mass fractions:

$$\rho = \alpha_g \rho_g + (1 - \alpha_g)\rho_l\,, \tag{4}$$

$$\mu = \alpha_g \mu_g + (1 - \alpha_g)\mu_l\,. \tag{5}$$

In the VOF multiphase model, the single energy equation is also shared between the liquid and vapour phases:

$$\frac{\partial}{\partial t}(\rho E) + \nabla \cdot (\vec{v}[\rho E + P]) = \nabla \cdot \left((k + k_t)\nabla T\right) + S_E, \tag{6}$$

where the energy E is treated as mass-averaged value

$$\left.\begin{aligned} E &= \frac{\alpha_g \rho_g E_g + \alpha_l \rho_l E_l}{\alpha_g \rho_g + \alpha_l \rho_l} \\ E_g &= h_g - \frac{P}{\rho_g} + \frac{\vec{v}^2}{2} \\ E_l &= h_l - \frac{P}{\rho_l} + \frac{\vec{v}^2}{2} \end{aligned}\right\}, \tag{7}$$

and liquid and vapour phase enthalpies h_l and h_g are based on the specific heats for liquid and gas phases and the shared temperature field. The source term S_E in energy Eq. (6) represents the volumetric heat source which is explicitly modelled as:

$$S_E = \dot{m}\, L\,, \tag{8}$$

where $\dot{m} = \dot{m}_{lg} - \dot{m}_{gl}$ is the mass transfer rate due to evaporation/condensation, numerically indicating positive mass transfer rate when evaporation occurs (i.e. $\dot{m}_{gl} = 0$) or negative mass transfer rate when condensation occurs (i.e. $\dot{m}_{lg} = 0$). And L is the latent heat of vaporization/condensation (see section 3.1.2 for details).

Species transport Eq. (9) is solved for NH_3 specie in the gas phase while the mass fraction for air is calculated using Eq. (10):

$$\frac{\partial}{\partial t}(\alpha_g \rho_g y_{NH_3}) + \nabla \cdot (\alpha_g \rho_g \vec{v}_g y_{NH_3}) = -\nabla \cdot \alpha_g \vec{J}_{NH_3} + \dot{m}_{lg} - \dot{m}_{gl}\,, \tag{9}$$

$$y_{air} = 1 - y_{NH_3}. \tag{10}$$

3.1.2. Phase change sub-model

The multiphase CFD model in this study utilizes Lee's model to describe mass transfer between liquid and gas phases, i.e., liquid ammonia evaporation and ammonia vapour condensation [22]. Lee's model is based on the fundamental idea that evaporation occurs when the liquid temperature rises above the

saturation temperature, i.e., boiling temperature at corresponding pressure, and condensation occurs when the vapour temperature falls below the saturation temperature Drop of gaseous ammonia pressure during venting process results in decrease of ammonia boiling temperature and when the boiling temperature falls below liquid ammonia temperature it triggers flash boiling. The mathematical form of the volumetric mass change rate source terms in Eqs. (1) and (9) is depicted by Eqs. (11a) and (11b):

$$\dot{m}_{lg} = \frac{r\,\alpha_g\,\rho_g\,(T_l - T_{sat})}{T_{sat}} \qquad if\ T_l > T_{sat}\ (evaporation), \tag{11a}$$

$$\dot{m}_{gl} = \frac{r\,\alpha_g\,\rho_g\,(T_{sat} - T_g)}{T_{sat}} \qquad if\ T_{sat} > T_g\ (condensation). \tag{11b}$$

The empirical coefficient r plays role of time relaxation parameter and influences the rate of evaporation and condensation. This empirical parameter includes the effect of unresolved phenomena such as size and number of bubbles influencing the contact surface between liquid and gas phases in the control volume, etc. There is no general agreement on the value of this coefficient and in the past authors varied it in wide limits between 10^{-3} and 10^{7} in order to reproduce experimental results [23–28]. In this study the value of this time relaxation parameter was determined using the inverse problem method, i.e., by selecting the value that closely reproduces the experimental data, i.e., the mass of ammonia of 300 kg released in 460 s and the corresponding pressure drop in the vessel.

The saturation temperature used in the mass transfer calculations in Lee's phase change model (see Eqs. (11a) and (11b)) is interpolated based on tabulated input given as a function of pressure based on NIST data [30]. Equation (12) presents the same data as a correlation for reader's convenience (applicable between pressure range 0.1 and 0.70 MPa abs):

$$T_{sat}\ (K) = -8.118 \cdot 10^{-11} \cdot P^2 + 1.384 \cdot 10^{-4} \cdot P + 229.1\ . \tag{12}$$

The latent heat of ammonia evaporation-condensation in Eq. (8) is a function of temperature and was as well interpolated from given tabulated input from NIST data [29]. Equation (13) provides the same data in the form of correlation (applicable between temperature range 239 and 287.15 K):

$$L\ (J/kg) = -9.511 \cdot T^2 + 1645 \cdot T + 1522000\ . \tag{13}$$

3.4. Computational domain and mesh

Figure 2(a) shows the isometric view of calculation domain consisting of the liquid ammonia tank, connecting pipe with valves and release nozzle, and the area simulating ambient atmosphere around the nozzle. The side view of the liquid ammonia tank model with the pipe is shown in the zoomed-in area in Fig. 2(b). The ammonia storage tank was modelled as a horizontal cylinder with dimensions corresponding to the experimental tank. In the computational domain, the 3/2-inch manual valve was positioned 0.55 m from the tank considering the tank insulation wall equal to 0.55 m which was not a part of the calculation domain. The manual valve is then connected to a 10.4 m long pipe that links to the release system, which consists of another 3/2-inch manual valve and a 50 mm internal diameter release nozzle that is 12.75 m away from the storage tank internal shell. For simplicity, the pipe connected to the manual valve was considered as a straight pipe instead of the bends as shown in the experimental set up. The part of domain mimicking the atmosphere has dimensions $L \times W \times H$=30×20×10 m. The dispersion analysis is out of the scope of this paper, yet the computational domain is designed to simulate the correct conditions at the pipe exit: release pipe is protruded 0.5 m inside the surroundings part of the domain so that the pressure boundaries do not affect air entrainment in the ammonia vapour stream.

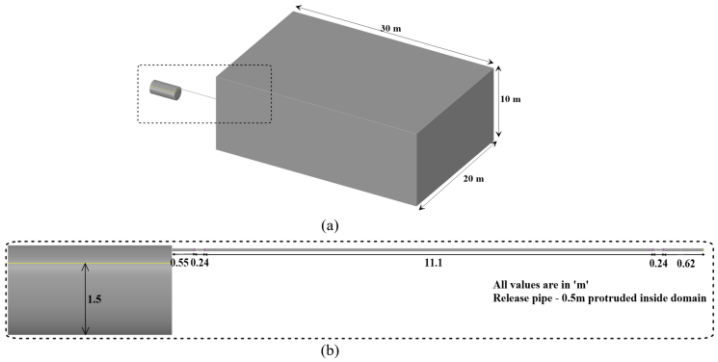

Figure 1. (a) Iso-metric view of geometry of the computational domain, (b) zoom-in area of liquid ammonia tank and connected piping system

Although the experimental report does not mention the tank material, in this numerical study we assume the inner tank shell was made of carbon steel, which is the most used material for liquid ammonia storage at elevated pressures [28]. The tank has an insulation thickness of 0.55 m of unnamed material. Thus in the simulations, the insulation material was assumed to be polyurethane foam as commonly used for insulation of ammonia storage tanks, see [29,30]. It's important to note that the experimentalists did not monitor the tank's fill level before each test. Instead, they only recorded the maximum fill level among 15 test cases as 1.5 m from the tank bottom which approximately corresponds to 85% filled tank. As the simulated test was first in the test series in this study it was assumed that the liquid height corresponded to the maximum fill level reported.

Figure 3 shows numerical mesh on the boundaries of the entire calculation domain and the ammonia storage tank. The total number of control volumes (CVs) in the computational domain is 419,953 with less than 20% of the total CVs located in the part of the domain mimicking ambient atmosphere. A grid expansion ratio of 1.1 was applied near to the pipe exit and ratio of 1.2 was used in the far field from the nozzle. The minimum orthogonal quality of mesh is 0.58 with an average quality 0.95 out of possible 1.00.

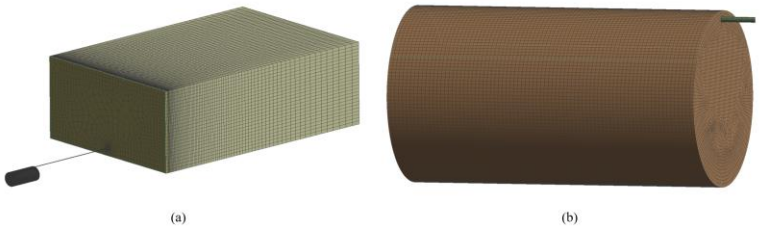

Figure 3. (a) General view of computational domain with boundary mesh, (b) close-up NH_3 storage tank and tank mesh

3.5. Numerical details and material properties

The simulations are performed using ANSYS Fluent 2020 R2. The pressure-based solver with SIMPLEC pressure-velocity coupling algorithm is utilized. Density of ammonia vapor has been calculated using ideal gas EoS as the ammonia storage pressure of 0.604 MPa in Test No.1 is significantly below the threshold of 10 MPa for using real gas EoS [31,32]. It is also worth mentioning, that the comparison of the use of ideal gas EoS or real gas EoS does not show any change in the pressure dynamics in the currently developed model. Density of liquid ammonia was modelled as a function of temperature. The thermal conductivity, specific heat capacity and viscosity of liquid and vapour ammonia has been defined as a function of temperature based on the NIST data [27]. The correlations for liquid and vapour ammonia physical properties used in simulations (applicable in the range of temperatures 239 and 287.15 K) are shown in Table 1.

Table 1. Correlations used for physical properties of liquid and vapour ammonia.

Physical property	Correlation as function of temperature
Thermal conductivity	$k_v = 6.892 \cdot 10^{-7} \cdot \mathrm{T}^2 - 2.317 \cdot 10^{-4} \cdot \mathrm{T} + 3.548 \cdot 10^{-2}$ $k_l = -7.977 \cdot 10^{-6} \cdot \mathrm{T}^2 + 2.405 \cdot 10^{-3} \cdot \mathrm{T} - 0.4609$
Specific heat capacity	$C_{p_v} = 9.369 \cdot 10^{-2} \cdot \mathrm{T}^2 - 35.95 \cdot \mathrm{T} + 5527$ $C_{p_l} = 3.444 \cdot 10^{-3} \cdot \mathrm{T}^2 - 13.4 \cdot \mathrm{T} + 5700$
Viscosity	μ_v=1.985$\cdot 10^{-11} \cdot \mathrm{T}^2 + 1.992 \cdot 10^{-8} \cdot \mathrm{T} + 2.147 \cdot 10^{-6}$ $\mu_l = 2.163 \cdot 10^{-8} \cdot \mathrm{T}^2 - 1.367 \cdot 10^{-5} \cdot \mathrm{T} + 2.2284 \cdot 10^{-3}$

3.6. Initial and boundary conditions

Initial temperature in the pressure vessel and vent pipe containing ammonia vapour was 9.5℃ while in the part of domain mimicking ambient conditions it was equal 14℃ following the reported experimental mean ambient temperature. Initial temperature in the liquid phase was equal to the saturation temperature which was a function of pressure as described by eqn. 12. Initial pressure in the storage tank was set as 0.604 MPa, which corresponds to saturated conditions at 9.5℃, and initial pressure distribution through the liquid ammonia accounted hydrostatic pressure. At initial moment the storage tank was assumed to be filled with liquid ammonia up to 1.5 m from the bottom; the top portion of the tank was assumed to be filled with ammonia vapour; in the vent pipe connected to the tank and before the second valve (located approximately 11.8 m from the tank) gaseous phase volume fraction was equal $\alpha_v = 1.0$, ammonia mass fraction $y_{NH3} = 1.0$ and pressure was equal 0.604 MPa. The second valve, exit pipe section (having length 0.62 m) and the part of the domain mimicking ambient atmosphere had gaseous phase volume fraction $\alpha_v = 1.0$ and air mass fraction $y_{air} = 1.0$; pressure was equal to one atmosphere.

All walls including ground, tank, pipe and valves are modelled as non-slip and non-permeable boundaries. The ground was set as adiabatic wall while the remaining wall boundaries accounted for convective heat exchange with ambient atmosphere. Non-reflecting pressure boundary conditions with *P*= 0.101325 MPa abs is applied at the side and top surfaces of the domain part representing the ambient atmosphere. Pipe material before release system, which is mentioned as flexible pipe in the experimental paper [15], is considered as rubber hose since specific material information was not given. The tank material is set as carbon steel and the polyurethane foam insulation is modelled using Fluent "shell conduction" capability. Shell conduction allows modelling of heat transfer through multiple layers of materials of different properties without the actual necessity to mesh the walls in the computational domain. For tank walls, carbon steel was the first layer, i.e. layer in contact with the fluid inside, and polyurethane foam was the second layer.

4. RESULTS AND DISCUSSION

The pressure transient from simulation is shown in Fig. 4(a) for the full venting duration against the presumed experimental beginning pressure of 0.604 MPa and the experimentally recorded final pressure of 0.18 MPa. The beginning pressure of 0.604 MPa was assessed by parametric studies to determine the correct initial conditions. In the current simulation, the value of time relaxation parameter was chosen as $r = 7 \cdot 10^{-3}$ s^{-1} based on sensitivity analysis to closely match the available experimental data. The simulated depressurisation dynamics closely matches the experiment final pressure with only 4.3% deviation. In the numerical study, the total mass released during 460 s was 308.54 kg, which is just 2.81% deviation from the experimentally reported mass of 300 kg.

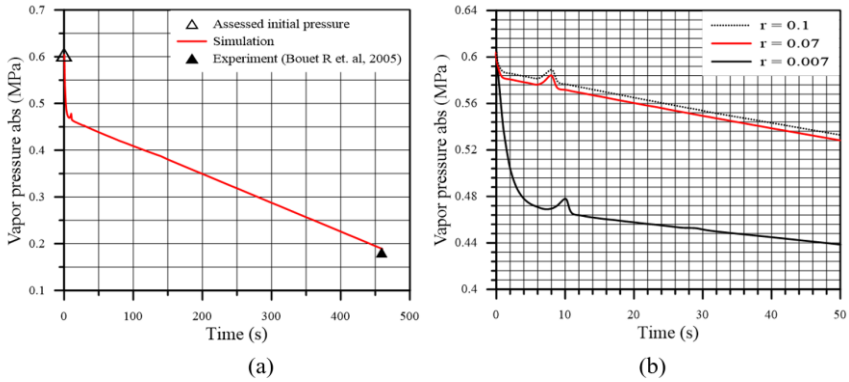

Figure 4. (a) Comparison of simulated depressurisation dynamics against experiment, (b) Influence of time relaxation parameter on depressurisation dynamics

The time relaxation parameter *r*=0.007 was selected in order to obtain the total released mass close to 300 kg while achieving final pressure close to the experimental target of 0.18 MPa (see Figure 4(a)). The released mass with *r*=0.1 and *r*=0.07 parameters was, respectively, 20.34% and 19.8% greater than with *r*=0.007 during the same venting time period. Figure 4(b) demonstrates the CFD model's sensitivity to time relaxation parameter '*r*' during the initial depressurisation period which is the basis for choosing the value '*r*' for the whole venting period of 460 seconds.

Figure 5 illustrates the time variations in the vapour pressure, temperature of the gaseous and liquid phases, saturation temperature, venting flowrate, and the mass evaporated as a result of the phase change in response to depressurization during the tank venting process. To clearly understand the underlying phenomenon causing the PRP, the analysis was done based on equation of state for gas phase $P \cdot V_U = (M_U/M_W)\, RT$. Different stages of PRP are explained below.

Stage 1 (A-B): at point A, see Fig. 5(a), the vessel is at its initial state prior to the venting process containing saturated liquid with saturated vapour in ullage space. The tank venting process results in rapid depressurisation causing the pressure to drop from its initial pressure P_A to pressure P_B resulting in the formation of a superheated liquid. Initial phase of boiling in bulk liquid is observed during this period, gaseous bubbles are formed but not yet sufficient to significantly add vapour to the tank ullage space. The liquid/vapour interface rises due to the formation and hold up of vapour bubbles. Figure 5(b) indicates that volume of ullage space (i.e. gaseous ammonia) decreases during the initial depressurisation period. This, however, does not lead to increase of pressure because mass of gas in ullage, shown in the same Fig. 5(b), decreases drastically too having dominating effect on pressure dynamics compare to decrease of ullage volume. During this stage, the temperature of the gaseous phase first drops due to adiabatic expansion. As venting proceeds, the evaporated ammonia at relatively higher saturation temperature starts to enter ullage space thus making the temperature of the initial gas phase to increase again, see Fig. 5(d).

Stage 2 (B-C): after the pressure reaches value P_B, the vessel pressure starts to increase again after $t_B = 6.5$ s and reaches the maximum recovered pressure P_C at $t_C = 10$ s. This phenomenon is stated as PRP. Time t_B here is termed as bubble rise time, i.e. the time duration essential for the bubbles generated in the liquid after boiling was triggered by depressurisation to rise through the bulk fluid to the liquid surface and break through the liquid/vapour interface into the tank ullage space. The obtained in CFD simulations bubble rise time was compared against results of analytical analysis based on the bubble velocity expressions developed by DIERS [35]:

$$U_{bubble} = 1.53 \left\{ \frac{\sigma \cdot g \cdot [\rho_l - \rho_v]}{{\rho_l}^2} \right\}^{0.25} . \quad (14)$$

The analytical equation (14) utilises the density of liquid and vapor, and the surface tension parameter corresponding to the initial tank pressure and temperature taken from NIST database [27] providing a calculated bubble rise time of 7.14 s to travel through 1.5 m of liquid ammonia depth. This is in close agreement with the numerically simulated bubble rise time of 6.5 s after which the pressure starts to recover thus proving the validity of CFD model to predict PRP characteristics. At this stage the mass

rate of evaporated ammonia entering the ullage from liquid/gas interface, indicated by mass entering ullage in Fig. 5(c), starts to exceed the mass being vented. As more vapour is generated due to boiling than can be vented the pressure starts to recover. It is worth noting that the superheat temperature difference (see Fig. 5(d)), which is proportional to depressurisation rate, sharply decreases as pressure rises during the PRP period.

Stage 3 (C-D and after): Following the previous stage, mass vented and mass generated due to evaporation continue to balance each other thus attaining a quasi-steady state (see Fig.5(c)). The average temperatures for both gas and liquid phase in the vessel gradually decreases (Fig. 5(d)) as the heat of vaporisation is absorbed during boiling. The combined effects of the temperature reduction and increase of ullage volume causes the pressure to continue to decrease even though vapour mass entering ullage and vapour mass vented are in a quasi-equilibrium. It should be noted that ullage volume (Fig. 5(b)) is calculated based on the volume of gas above the liquid/gas interface which in the computational model is defined as iso-line $\alpha_l = 0.5$.

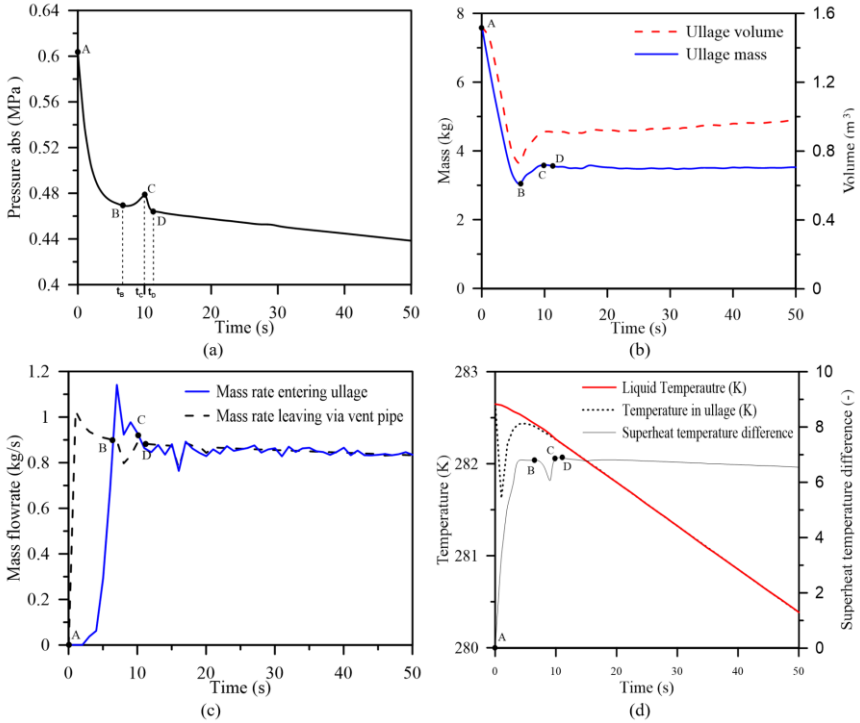

Figure 5. (a) Pressure recovery dynamics, (b) ammonia volume and mass dynamics in ullage space, (c) vented and evaporated ammonia mass flow rate, (d) time variation of superheat temperature difference, liquid and gas phase temperature

Figure 6 shows liquid phase VOF in central cross section of the ammonia tank, which illustrates liquid motion and boiling behaviour during the same period between 0 and 50 s. The results of the simulation show that boiling does not begin at the tank walls but rather occurs through the whole liquid bulk, suggesting that pressure drop due to venting resulted in homogeneous nucleation, i.e. the formation of bubbles as a result of superheated ammonia state without influence of tank walls acting as bubble nucleation sites. It can be seen from Fig. 6 that liquid level increases (i.e. liquid swell / 'piston effect') due to generation and hold-up of vapour bubbles as a result of flash boiling. Despite the occurrence of the "piston effect," it is clear from prior analysis that the PRP is primarily driven not by gas compression in ullage but by changes in ullage mass and the mass generated due to flash boiling.

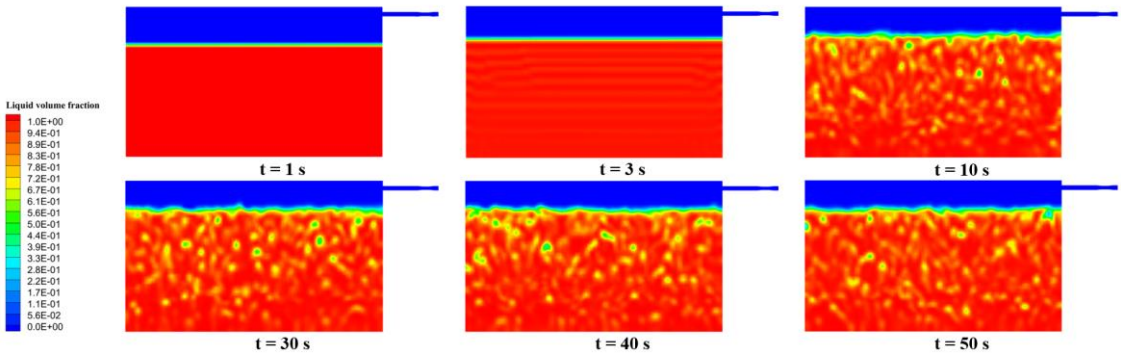

Figure 6. Dynamics of liquid phase volume fraction with time (boiling due to flash evaporation)

Figure 7 shows sensitivity of simulated pressure dynamics to grid size and time step during the initial highly transient depressurisation phase when PRP is observed. Three different numerical grids (coarse – 228,926 CVs, intermediate – 419,153 CVs, and fine – 786,983 CVs) were used for grid sensitivity analysis during depressurisation period where PRP was observed as shown in Fig. 7(a). The intermediate mesh was selected for simulations as the peak pressure difference at t=10 s between intermediate and fine mesh sizes is only 0.63% and pressure dynamics is practically coinciding for all three meshes during the rest of simulation period. The time step sensitivity analysis as shown in fig. 7(b) demonstrates a relative difference of only 0.74% between the pressure peaks during PRP period obtained with time step sizes Δt=0.003s and Δt=0.01s, which allowed the authors to use time step size Δt=0.01s during the initial depressurization phase.

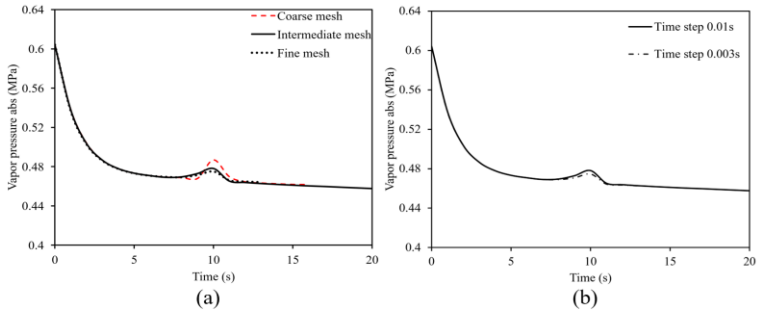

Figure 7. (a) Grid sensitivity analysis, (b) time step sensitivity analysis

5. CONCLUSION

The originality of this work is in the investigation for the first time of the pressure recovery phenomenon (PRP) and the flash boiling behaviour of liquid ammonia during tank depressurisation. Simulation results for the complex two-phase flow with simultaneous boiling and condensation under reducing pressure are compared against the INERIS experimental data for large scale ammonia evaporation and release study. The test trial focusing on pure gaseous release from pressurised ammonia storage system at 9.5 °C and 0.604 MPa was used for computational modelling. The CFD model adopted Volume of Fluid (VOF) method for phase interaction and Lee evaporation/condensation model to simulate flash boiling of liquid ammonia. The CFD model predicted the bubble rise time in close agreement with analytical calculations for bubble rise time.

The significance of this work is in the development and implementation of a multi-phase CFD model able to predict flashing phenomena and pressure recovery characteristics of liquid ammonia systems subjected to tank venting operation. The model accounts both the effect of boiling and the effect of condensation during tank depressurisation. Analysis of simulation results provided insight and understanding of flash boiling: it proved that the mechanism underlying pressure recovery phenomenon is the mass entering the ullage due to flash boiling after a delay indicated by bubble rise time and not

the liquid swell acting as a "piston effect". The results of the simulations allow designing inherently safer tank management strategies for liquid ammonia storage tanks.

The rigour of this research is in the thorough comparison of the developed CFD model against the available experimental data on the depressurisation of horizontal liquid ammonia tank. The CFD model simulations accurately simulated the PRP and the associated phenomenon of pressure recovery with accurate understanding of bubble rise time. Future work will focus on the development of a CFD model capable of predicting hazard distances based on toxicity and flammability limits for large scale dispersion of ammonia in open atmosphere based on the inputs from current results.

ACKNOWLEDGEMENTS

This research was funded by Engineering and Physical Sciences Research Council (EPSRC) of the UK for funding through the Centre for Doctoral Training in Sustainable Hydrogen "SusHy", grant number EP/S023909/1. The authors are very grateful for the discussions with Mr H Ebne-Abbasi, Dr D Cirrone and Dr T Kangwanpongpan which helped during the CFD model development. The authors would like to acknowledge EPSRC for funding the project Kelvin-2 "Tier 2 High-Performance Computing Services" (EP/T022175/1).

REFERENCES

[1] Kojima Y, Liquid Ammonia for Hydrogen Storage. In *Ammonia energy conference*, 2014.

[2] Kashkarov S, Li Z, Molkov V. Blast wave from a hydrogen tank rupture in a fire in the open: Hazard distance nomograms. *International Journal of Hydrogen Energy*, **45**, No. 3, 2020, pp. 2429–2446.

[3] Eckhoff, R.K., Boiling liquid expanding vapour explosions (BLEVEs): A brief review, *Journal of Loss Prevention in the Process Industries*, **32**, 2014, pp.30-43.

[4] Watanabe, T., Nakano, A., Kambara, K., Tokunaga, K., Shiigi, T. and Shimojima, K., 2022. Phenomena of Liquid Nitrogen Flashing under Rapid Depressurizations. The International Journal of Multiphysics, **16**, No. 3, pp.223-233.

[5] Takeda, M., Usui, T. and Maekawa, K., 2019, April. Study on boiling behaviour of pressurized liquid nitrogen under rapid depressurization. In *proceedings of 27th International Cryogenics Engineering Conference and International Cryogenic Materials Conference* (ICEC-ICMC 2018) 3–7 September 2018, Oxford, United Kingdom

[6] Watanabe T, Hanaoka Y, Tokura I. Flashing phenomena of depressurized liquid nitrogen in a pressure vessel: Part 2: Mist formation and behaviour of the liquid surface in the early depressurization process. Heat Transfer - Japanese Research, **27**, No. 5, 19983, pp. 27–35.

[7] Bentz, M. and Wilkinson, C., 1975. Experimental study of flash boiling in liquid nitrogen. In 19th Joint Propulsion Conference (p. 1378).

[8] Saury D, Harmand S, Siroux M. Flash evaporation from a water pool: Influence of the liquid height and of the depressurization rate, *International Journal of Thermal Sciences*, **44**, No. 10, pp. 953–965.

[9] Shang Q, Tian Z, Wang S, Hua M, Pan X, Shi S, et al. Experimental research on the two-phase explosive boiling mechanism of superheated liquid under different leakage conditions. Applied Thermal Engineering, 216, 2022, p. 119080.

[10] Barbone R., Frost D.L, Makris A., Nerenberg J. Explosive Boiling of a Depressurized Volatile Liquid. IUTAM Symposium on Waves in Liquid/Gas and Liquid/Vapor Two phase systems, 1994, p. 315–320.

[11] Hanoka Y, Maeno K, Zhao L, Heymann G. A study of liquid flashing phenomenon under rapid depressurization, *JSME International Journal Ser.2*, **33**, No. 2,1990, pp. 276–282.

[12] Park RJ, Kim SB, Hong SW, Kim HD. Detailed evaluation of coolant injection into the reactor vessel with RCS depressurization for high pressure sequences, *Nuclear Engineering and Design*, **239**, No. 11, pp. 2484–2490.

[13] Tani, K., Himeno, T., Sakuma, Y., Watanabe, T., Kobayashi, H., Toge, T., Unno, S., Kamiya, S., Muragishi, O. and Kanbe, K, Pressure recovery during pressure reduction experiment with

large-scale liquid hydrogen tank. *International Journal of Hydrogen Energy*, **46**, No. 57, 2021, pp.29583-29596.
[14] Ma Q., Zhong M., Guo Y., You J., He Y., Chen J. and Zhang Z, Study on the characteristic of boiling expansion process of superheated LPG and its vapor cloud explosion, *Journal of Loss Prevention in the Process Industries*, **78**, 2022, p.104831.
[15] Tian, Z., Shang, Q., Pan, X., Zhang, R., Hua, M., Zhao, Y. and Jiang, J., Experimental study on explosive boiling mechanism of superheated liquid containing ethanol impurities under rapid depressurization, *Process Safety and Environmental Protection*, **168**, 2022 pp.443-453.
[16] Bouet R, Salvi O, Faucher B, AMMONIA Large-scale atmospheric dispersion tests, 2005, INERIS-France report No. INERIS-DRA-RBo-1999-20410.
[17] ANSYS. ANSYS Fluent Theory Guide, 2020.
[18] Wang X, Yao H, Li J, Wang Y, Zhu Y, Experimental and numerical investigation on heat transfer characteristics of ammonia thermosyphons at shallow geothermal temperature, *International Journal of Heat and Mass Transfer*, **136**, 2019, pp. 1147–1159.
[19] Zheng Y, Chang H, Chen J, Chen H, Shu S. Effect of microgravity on flow boiling heat transfer of liquid hydrogen in transportation pipes, *International Journal of Hydrogen Energy*, **44**, No. 11, 2019, pp. 5543–5550.
[20] Lee, W.H., Pressure iteration scheme for two-phase flow modelling. In multiphase transport: fundamentals, reactor safety, applications, 1980, pp.407-432.
[21] Wu HL, Peng XF, Ye P, Eric Gong Y. Simulation of refrigerant flow boiling in serpentine tubes. Int J Heat Mass Transf 2007;50:1186–95.
[22] Yang Z, Peng XF, Ye P. Numerical and experimental investigation of two-phase flow during boiling in a coiled tube. Int J Heat Mass Transf 2008;51:1003–16.
[23] De Schepper SCK, Heynderickx GJ, Marin GB. Modelling the evaporation of a hydrocarbon feedstock in the convection section of a steam cracker. Comput Chem Eng 2009;33:122–32.
[24] Teng L, Liu X, Bian J, Li Y, Lu C. A homogeneous relaxation model for multi-phase CO2 jets following the release of supercritical CO2 pipelines. J Nat Gas Sci Eng 2020;84:103609.
[25] You Y, Wang G, Guo C, Jiang H. Study on mass transfer time relaxation parameter of indirect evaporative cooler considering primary air condensation. Appl Therm Eng 2020;181:115958.
[26] Zhang J, Li W. Numerical study on heat transfer and pressure drop characteristics of R410A condensation in horizontal circular mini/micro-tubes. Can J Chem Eng 2016;94:1809–19.
[27] NIST chemistry webbook. Thermophysical properties of fluid systems. 2021 https://webbook.nist.gov/chemistry/fluid/ [Accessed 4 November 2021]
[28] Pasman H. Industrial Processing Systems, Their Products and Hazards. Risk Analysis and Control for Industrial Processes - Gas, Oil and Chemicals, Elsevier; 2015, p. 1–31.
[29] Abdulla Y, Narasimha Y. Successful inspection of two large ammonia storage tanks. Process Safety Progress 2009;28:45–59. https://doi.org/10.1002/prs.10278.
[30] Shah JM. Refrigerated ammonia storage tanks. Plant/Operations Progress 1982;1:90–3.
[31] Molkov V. Fundamentals of Hydrogen Safety Engineering I. 2012.
[32] Tolias IC, Giannissi SG, Venetsanos AG, Keenan J, Shentsov V, Makarov D, et al. Best practice guidelines in numerical simulations and CFD benchmarking for hydrogen safety applications. Int J Hydrogen Energy 2019;44:9050–62.
[33] DIERS Technology Report, Emergency Relief Systems for Runaway Chemical Reactions and Storage Vessels: A Summary of Multiphase Flow Methods. Illinois: 1984.